Analysis and computation of a least-squares method for consistent mesh tying. [1]

David Day and Pavel Bochev *

Computational Mathematics and Algorithms, Sandia National Laboratories
P.O. Box 5800, MS 1320, Albuquerque NM 87185-1320

Abstract

In the finite element method, a standard approach to mesh tying is to apply Lagrange multipliers. If the interface is curved, however, discretization generally leads to adjoining surfaces that do not coincide spatially. Straightforward Lagrange multiplier methods lead to discrete formulations failing a first-order patch test [18].

This paper presents a theoretical and computational study of a least-squares method for mesh tying [4], applied to the partial differential equation $-\nabla^2\phi + \alpha\phi = f$. We prove optimal convergence rates for domains represented as overlapping subdomains and show that the least-squares method passes a patch test of the order of the finite element space by construction. To apply the method to subdomain configurations with gaps and overlaps we use interface perturbations to eliminate the gaps. Theoretical error estimates are illustrated by numerical experiments.

Key words: finite elements, mesh tying, least-squares, first-order elliptic systems
PACS: 65F10, 65F30

1 Introduction

Mesh tying, or domain bridging methods [3, 4, 7, 8, 16] are the opposite of domain decomposition (DD) [23]. A DD method solves a boundary value problem

* Corresponding author.
Email addresses: dmday@sandia.gov (David Day), pbboche@sandia.gov (Pavel Bochev).

[1] Sandia is a multiprogram laboratory operated by Sandia Corporation, a Lockheed-Martin Company, for the United States Department of Energy's National Nuclear Security Administration under contract DE-AC-94AL85000.

using subdomains formed by clustering finite elements from a given discretization of a domain Ω. A mesh tying method solves the same problem by using a discretization of Ω, composed of subdomains that were meshed completely independently. The weak problem is obtained by joining subdomain problems through a suitable variational principle.

The simplest nontrivial case of mesh tying is as follows. Assume that Ω is an open bounded domain with Lipschitz continuous boundary Γ, composed of two subdomains; $\overline{\Omega}_1 \cup \overline{\Omega}_2 = \overline{\Omega}$ and $\Omega_1 \cap \Omega_2 = \emptyset$. The *interface* between the two domains, $\sigma = \overline{\Omega}_1 \cap \overline{\Omega}_2$, is non-empty, connected set. We want to solve numerically the elliptic boundary value problem

$$\begin{cases} -\nabla \cdot \mathbf{A}\nabla\phi + \alpha\phi = f \quad \text{in } \Omega \\ \qquad\qquad \phi = h \quad \text{on } \Gamma \end{cases}, \tag{1}$$

using independently defined finite element partitions of Ω_1 and Ω_2, with boundary conditions imposed on each $\Gamma_i = \Gamma \cap \overline{\Omega}_i$

The main reason to use this computational setting is modeling and simulation of complex engineering structures in which the bottleneck, as measured in calendar time, is mesh generation. One example is certification of aerospace structures where creating a monolithic mesh is hugely impractical and time consuming. In such cases, for practical and efficiency reasons, grid generation on Ω is replaced by independent meshing of its subdomains [3, 4, 8, 10, 16, 19, 20]. Other examples that lead to mesh tying settings include transmission, contact, and domain-bridging problems [1, 6, 15, 17].

1.1 Specifics of mesh tying

In mesh tying Ω is first partitioned into subdomains and then each subdomain is discretized independently. Let Ω_i^h denote a discretization of Ω_i, $i = 1, 2$. The discrete subdomains induce approximations Γ_1^h, Γ_2^h, σ_1^h and σ_2^h of Γ_1, Γ_2 and the interface σ, respectively. The discretization of Ω is given by $\Omega^h = \Omega_1^h \cup \Omega_2^h$. In mesh tying there are two basic configurations for the discrete interfaces σ_1^h and σ_2^h. The first one is when the adjoining surfaces spatially coincide, $\sigma_1^h = \sigma_2^h = \sigma^h$. This configuration arises from cutting a domain into simpler subdomains to improve efficiency of the mesher, a practice often used with Sandia's meshing tool CUBIT. An example of a CUBIT hex mesh obtained in this way is shown in Figure 1. In this example the shape of Ω is such that planar and curved interfaces can be easily matched. The general case, $\sigma_1^h \neq \sigma_2^h$, arises when the grids on the two sides of a curved interface σ cannot be easily

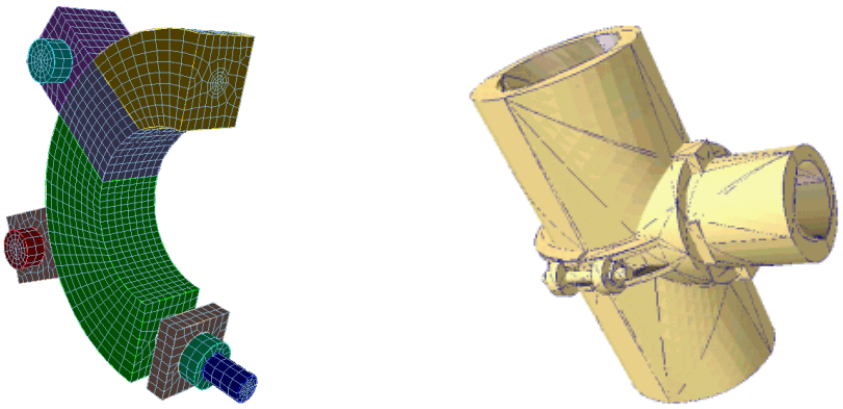

Fig. 1. The left plot shows an example of mesh tying configuration with matching interfaces. The right plot is an example of a domain with more complicated curved interfaces that may lead to $\sigma_1^h \neq \sigma_2^h$.

matched [2] . Typically, this happens with more complex shapes, such as the object shown on the right in Figure 1, transmission problems where discontinuous coefficients naturally lead to curved interfaces, and contact problems where the interface is between different bodies. In contrast, in domain decomposition methods [23], the discrete domain Ω_h is determined first, and the subdomains are defined *afterwards*. As a result, in these methods the adjoining interfaces always coincide, $\sigma_1^h = \sigma_2^h = \sigma^h$.

A minimal requirement for any mesh-tying or domain bridging method is a consistency condition called *patch test*. In addition to consistency, patch tests are used in practice for verification, and to identify discretizations that are nonconvergent or that cause impulse waves through the interface to disperse artificially. A method passes a patch test of order k if it can recover any solution of (1) that is a polynomial of degree k. When $\sigma_1^h \neq \sigma_2^h$ mesh tying methods based on Lagrange multipliers experience difficulties and naively defined schemes fail even a first-order patch test, see [18] for an example.

Several approaches have been proposed to address this problem in both two and three dimensions. Surface coupling methods [8–12, 18] start by selecting one of the non-matching interfaces as a master and the other as a slave surface. The approach of [10–12] defines Lagrange multipliers on the slave surface and

[2] Finite element methods routinely replace curved boundaries Γ by polyhedral approximations Γ^h, but replacing a curved interface σ by two spatially distinct discrete interfaces σ_1^h and σ_2^h is fundamentally different. Although either case is a 'variational crime' in the sense of [22, p.193], the former case leads to a perturbation of the original problem that can be estimated by the Strang's lemma [22, Lemma 4.1, p.186]. For polyhedral approximations the error in energy is $O(h^3)$; see [22, p.196]. In the latter case, the discrete computational domain $\Omega_1^h \cup \Omega_2^h$ has gaps and overlaps where the problem ceases to be well-defined. In the overlap regions the 'solution' is multiple valued, and in the voids it is undefined.

uses a projection operator from the master surface. The mesh tying methods considered in [8, 9, 17, 18] build additional mesh structures between the slave and master interfaces using tools that range from mesh imprinting to local L^2 projections. A disadvantage of these methods is that in order to maintain accuracy, typically six levels of uniform $3D$ mesh refinement are required near the boundary to pass the patch test approximately. The Generalized Lagrange Multiplier method of [19] avoids the mesh refinement but requires an *interface balancing procedure* to cancel out the signed ares of the gaps and overlaps.

Another approach that can be used for mesh tying is partition of unity methods (PUM) [1]. PUM represent a domain as an atlas of overlapping charts, and couple the volumes. The charts are subdomain meshes. For example, swapping charts adapts the mesh [16]. PUM methods with overlapping subdomain meshes are discussed in [2] for some 2D problems, and a related method [3] has been applied to plates, cracks and shells coupled to 3D models. The theoretical formulations of these methods is an active research area [15]. Note that [3, 15] are Mixed Galerkin formulations that use Lagrange multipliers in the overlap regions, and lead to indefinite linear systems.

Our approach [4] for dealing with non-matching interfaces utilizes least-squares principles and extends a least-squares finite element method (LSFEM) for transmission problems [6], where $\sigma_1^h = \sigma_2^h$, to mesh tying configurations where $\sigma_1^h \neq \sigma_2^h$. A least-squares functional is defined as the sum of the residuals of the differential equations measured in Sobolev space norms. As a result, such a functional always vanishes at the exact solution. By exploiting this property, a least-squares method for mesh tying is formulated that automatically passes a patch test of the same order as the finite element space employed in its definition. We start by perturbing the discrete interfaces until there are no void regions [3] between the subdomains. Then, least-squares principles for each subdomain are joined together by generalized jump terms defined on the overlap region [4] between the subdomains. This resembles the approach used in the Arelquin method [3] and in the domain bridging method [15]. However, by measuring residual energy and not physical energy, a least-squares func-

[3] Were the subdomains disjoint, the residual energy would have a space of minimizers of positive dimension (corresponding to the missing boundary conditions) and the coefficient matrix would be symmetric positive semi-definite.

[4] In our opinion, forcing the meshes to overlap is easier than attempting to remesh a complex body such as an aerospace structure. The perturbation required to overlap the meshes is similar in magnitude to the perturbations due to either r-adaptivity [13] or Lagrangian algorithms in which each individual node of the computational mesh follows the associated material particle during motion. Moreover, tools for assembling overlapping meshes already exist in the Overture package from Lawrence Livermore National Laboratory. Likewise, the composite overlapping grid method [7] for a collection of structured grids uses tools [20] to assemble overlapping substructure meshes.

tional may measure energy redundantly in subdomain intersections. This fact greatly simplifies our algorithm. In contrast, methods that minimize physical energy, subject to appropriate constraints on the interfaces, require special efforts to avoid counting energy twice in the overlap regions; see [3].

The contents of the paper are as follows. Section 1.2 reviews notation. The least squares method for mesh tying of [4] is formulated in Section 2. Section 3 presents analysis of the method. Numerical examples illustrating the consistency of the LSFEM are discussed in Section 4.

1.2 Notations

Our focus is on mesh tying for the case of non-matching interfaces. For clarity, throughout the paper we assume that Ω is such that $\Gamma^h = \Gamma$ and Ω_i^h match their continuous counterparts everywhere except along the interface σ, i.e.,

$$\Gamma_i^h = \Gamma_i \quad \text{but} \quad \sigma_1^h \neq \sigma_2^h \,,$$

where $\sigma_i^h = \partial\Omega_i^h / \Gamma_i^h$. The *void* and *overlap* regions between Ω_1^h and Ω_2^h are $\Omega_V = \Omega / (\overline{\Omega}_1^h \cup \overline{\Omega}_2^h)$ and $\Omega_O = \Omega_1^h \cap \Omega_2^h$, respectively. We assume that

$$\overline{\Omega} = (\overline{\Omega}_1^h / \Omega_O) \cup (\overline{\Omega}_2^h / \Omega_O) \cup \overline{\Omega}_O \cup \overline{\Omega}_V \,. \tag{2}$$

Variational settings will be discussed in terms of standard finite element notation. As usual, $L^2(\mathcal{D})$ is the Hilbert space of all square integrable functions defined over a domain $\mathcal{D}$. $H(\mathrm{div}, \mathcal{D})$ will stand for the Hilbert space of all functions in $(L^2(\mathcal{D}))^n$ with square integrable divergence, equipped with the norm

$$\|\mathbf{v}\|_{\mathrm{div},\mathcal{D}} = \left(\|\mathbf{v}\|_{0,\mathcal{D}}^2 + \|\nabla \cdot \mathbf{v}\|_{0,\mathcal{D}}^2 \right)^{1/2} .$$

For $k > 0$, $H^k(\mathcal{D})$ denotes the subspace of $L^2(\mathcal{D})$ that consists of all functions having square integrable derivatives up to order k. The space $H_0^1(\mathcal{D})$ contains all functions in $H^1(\mathcal{D})$ that vanish on $\partial\mathcal{D}$. In situations when $\partial\mathcal{D}$ is partitioned into two disjoint pieces Γ and σ, we will use $H_\Gamma^1(\mathcal{D})$ to denote all functions in $H^1(\mathcal{D})$ that vanish on Γ only. The inner product and norm on $H^k(\mathcal{D})$ are denoted $(\cdot,\cdot)_{k,\mathcal{D}}$ and $\|\cdot\|_{k,\mathcal{D}}$, respectively.

The trace of a function $\phi \in H^1(\mathcal{D})$ on a subset $\Gamma \subset \partial\mathcal{D}$ belongs to the space $H^{1/2}(\Gamma)$. Extensions by zero of functions in $H^{1/2}(\Gamma)$ to $H^{1/2}(\partial\mathcal{D})$ are in the space $H_{00}^{1/2}(\Gamma)$. The dual of this space is $H^{-1/2}(\Gamma)$; see [23, p.342], and $\langle\cdot,\cdot\rangle_\Gamma$ denotes the duality pairing. Given a vector field $\mathbf{v} \in H(\mathrm{div}, \mathcal{D})$, its normal component $\mathbf{v} \cdot \mathbf{n}$ belongs to $H^{-1/2}(\partial\mathcal{D})$; see [14, p.27].

To discuss LSFEM for mesh tying we need the tensor product space

$$\mathbf{H}^1 = \{\phi = (\phi_1, \phi_2) \,|\, \phi_i \in H^1(\Omega_i);\ i = 1, 2\}\,, \tag{3}$$

its subspace $\mathbf{H}^1_0$ consisting of pairs $(\phi_1, \phi_2) \in H^1_{\Gamma_1}(\Omega_1) \times H^1_{\Gamma_2}(\Omega_2)$ that vanish on Γ_i, and the space

$$\mathbf{H}(\mathrm{div}) = \{\mathbf{v} = (\mathbf{v}_1, \mathbf{v}_2) | \mathbf{v}_i \in H(\mathrm{div}, \Omega_i);\ i = 1, 2)\}. \tag{4}$$

The spaces $\mathbf{H}^1$ and $\mathbf{H}(\mathrm{div})$ equipped with the inner products

$$\langle \phi, \psi \rangle_1 = \sum_{i=1}^{2} (\phi_i, \psi_i)_{1,\Omega_i} \quad \text{and} \quad \langle \mathbf{u}, \mathbf{v} \rangle_{\mathrm{div}} = \sum_{i=1}^{2} (\mathbf{u}_i, \mathbf{v}_i)_{\mathrm{div},\Omega_i}\,,$$

and the induced norms $|||\cdot|||_1$ and $|||\cdot|||_{\mathrm{div}}$, are Hilbert spaces.

2 Least squares method for mesh tying

We assume the mesh tying setting described in §1. The mesh tying LSFEM proposed in [4] uses an equivalent first-order system form of (1). Assuming for simplicity that $\mathbf{A}$ is the identity and $\alpha = 1$, the reformulated equations are

$$\begin{cases} \nabla \cdot \mathbf{u}_i + \phi_i = f_i \quad \text{and} \quad \mathbf{u}_i + \nabla \phi_i = 0 \quad \text{in } \Omega_i \\ \qquad\qquad\qquad\quad \phi_i = 0 \quad \text{on } \Gamma_i \end{cases}; \quad i = 1, 2 \tag{5}$$

augmented with the interface conditions

$$\phi_1 = \phi_2 \quad \text{and} \quad \mathbf{u}_1 \cdot \mathbf{n}_1 + \mathbf{u}_2 \cdot \mathbf{n}_2 = 0 \quad \text{on } \sigma. \tag{6}$$

To motivate our approach, note that the interface conditions (6) are the "glue" applied to the interface σ to hold together the subdomain problems in (5). As a result, if $\sigma_1^h = \sigma_2^h$, the jump terms

$$[\psi] = \psi_1 - \psi_2 \quad \text{and} \quad [\mathbf{v}] = \mathbf{v}_1 \cdot \mathbf{n}_1 + \mathbf{v}_2 \cdot \mathbf{n}_2 \tag{7}$$

can be used to join together least-squares functionals for (5) in a well-posed LSFEM [6]. However, if $\sigma_1^h \neq \sigma_2^h$, the jump terms are undefined. On the other hand, if there's a sufficient overlap Ω_O between the subdomains, their least-squares functionals can be joined together by using the "generalized" jumps

$$\|\phi_1^h - \phi_2^h\|^2_{1,\Omega_O} \quad \text{and} \quad \|\mathbf{v}_1^h - \mathbf{v}_2^h\|^2_{\mathrm{div},\Omega_O}\,, \tag{8}$$

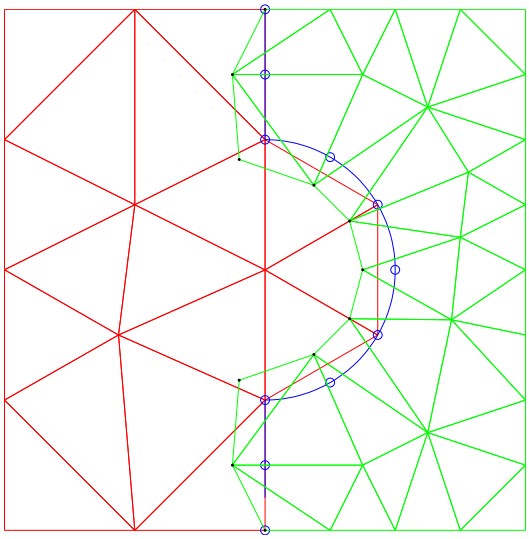

Fig. 2. Interface perturbations give subdomains with no gaps between them. The blue line is the interface σ. The domain $\Omega = [-1,1]^2$ has two overlapping subdomains. Only the interface nodes on the right (or green) domain are perturbed. The original interface node locations are marked with circles.

respectively, which replace the standard interface jump terms (7). Note that because a least-squares functional measures residual rather than physical energy, there's no need to subtract energy from Ω_O.

2.1 The mesh tying region

Our least-squares functional is defined in the case of overlapping regions, $\Omega_V = \emptyset$. Let σ^h denote the set of spatially coincident interface segments. We define the mesh tying "region" as

$$\Sigma^h = \Omega_O \cup \sigma^h = \overline{\Omega}_1^h \cap \overline{\Omega}_2^h. \tag{9}$$

In words, Σ^h is the union of the overlap region and any spatially coincident segments of the discrete interfaces. Note that σ^h may be empty but $\Omega_O \neq \emptyset$.

If Ω_i^h are such that $\Omega_V \neq \emptyset$ we proceed as follows to perturb the interface to close the voids. Bear in mind that in the case of polygonal domains and quasi-uniform meshes, the diameter of the overlap and void regions is $O(h^2)$. Let $N(\sigma_i^h)$ denote the set of all vertices on interface σ_i^h, $i = 1, 2$ that are not on the Dirichlet boundary Γ. For each vertex $\mathbf{z}_i \in N(\sigma_i^h)$ we consider a perturbation $\delta\mathbf{z}_i$ and define the perturbed subdomains $\widehat{\Omega}_i^h$ by changing $\mathbf{z}_i \in N(\sigma_i^h)$ to $\mathbf{z}_i + \delta\mathbf{z}_i$. Note that the only elements in $\widehat{\Omega}_i^h$ that differ from the elements in Ω_i^h are those that have a vertex on the interface. We assume that Ω_i^h are such that there exist perturbations $\delta\mathbf{z}$ with the following properties; see Figure 2:

(1) The void region, Ω_V, of the perturbed subdomains is empty.
(2) The overlap region $\widehat{\Omega}_O = \widehat{\Omega}_1^h \cap \widehat{\Omega}_2^h \neq \emptyset$ or if $\widehat{\Omega}_O = \emptyset$, then $\sigma_1^h = \sigma_2^h = \sigma^h$.
(3) All perturbed elements in $\widehat{\Omega}_i^h$ are non-degenerate.

The hypothesis that $\Omega_V = \emptyset$ is satisfied by defining Σ^h as in (9) but in terms of the perturbed subdomains. In most situations of practical interest, the conditions are easily met. The resulting overlap region Ω_O may not be simply connected. However, it is important to note that the purpose of the interface node perturbations is not to match [5] the interfaces (which in general is impossible), but only to eliminate the void region. In contrast, mesh imprinting/refining techniques tend to be more complicated, because they have to preserve the existing interfaces.

2.2 A least-squares principle for mesh tying

In what follows $\mathbf{H}^1$ and $\mathbf{H}(\mathrm{div})$ denote the spaces (3) and (4) defined with respect to Ω_1^h and Ω_2^h. Let $\mathbf{H}^h$ denote a finite element subspace of $\mathbf{H}^1 \times \mathbf{H}(\mathrm{div})$. We consider the following least-squares functional on $\mathbf{H}^h$:

$$\begin{aligned} J_h(\{\psi^h, \mathbf{v}^h\}; f) = \frac{1}{2}\Big(\sum_{i=1}^{2} \|\nabla \cdot \mathbf{v}_i^h + \psi_i^h - f_i\|_{0,\Omega_i^h}^2 + \|\mathbf{v}_i^h + \nabla \psi_i^h\|_{0,\Omega_i^h}^2 \\ + \frac{1}{h^{1+\varepsilon_0}} \int_{\sigma^h} [\psi^h]^2 \, ds + \frac{1}{h^{\varepsilon_1}} \int_{\sigma^h} [\mathbf{v}^h]^2 \, ds\Big) \\ + \omega_\phi \|\psi_1^h - \psi_2^h\|_{1,\Omega_O}^2 + \omega_{\mathbf{v}} \|\mathbf{v}_1^h - \mathbf{v}_2^h\|_{\mathrm{div},\Omega_O}^2 \,, \end{aligned} \tag{10}$$

where σ^h is the set from (9). In other words, we define the mesh-tying LSFEM by gluing subdomain LSFEMs using the standard jump terms (7) on σ^h and the generalized jumps (8) on Ω_O. The weights ω_ϕ and $\omega_{\mathbf{v}}$ are positive real numbers that are independent of the mesh size h. The least-squares principle for (10) is

$$\min_{(\psi^h, \mathbf{v}^h) \in \mathbf{H}^h} J_h(\{\psi^h, \mathbf{v}^h\}; f). \tag{11}$$

The finite element approximation $\{\phi^h, \mathbf{u}^h\} \in \mathbf{H}^h$ solves the Euler equation

$$B_\Sigma^h(\{\phi^h, \mathbf{u}^h\}; \{\psi^h, \mathbf{v}^h\}) = F_\Sigma^h(\{\psi^h, \mathbf{v}^h\}) \quad \forall \{\psi^h, \mathbf{v}^h\} \in \mathbf{H}^h. \tag{12}$$

[5] In some cases, perturbations such that $\sigma^h \neq \emptyset$, or even $\Sigma^h = \sigma^h$ are available.

The bilinear form and functional in (11) are given by

$$
\begin{aligned}
&B^h_\Sigma(\{\phi^h,\mathbf{u}^h\};\{\psi^h,\mathbf{v}^h\})\\
&\quad=\sum_{i=1}^{2}\left(\nabla\cdot\mathbf{u}_i^h+\phi_i,\nabla\cdot\mathbf{v}_i^h+\psi_i\right)_{0,\Omega_i^h}+\left(\mathbf{u}_i^h+\nabla\phi_i^h,\mathbf{v}_i+\nabla\psi_i\right)_{0,\Omega_i^h}\\
&\quad+\frac{1}{h^{1+\varepsilon_0}}\int_{\sigma^h}[\phi^h][\psi^h]\,ds+\frac{1}{h^{\varepsilon_1}}\int_{\sigma^h}[\mathbf{u}^h][\mathbf{v}^h]\,ds\\
&\quad+\omega_\phi\left(\phi_1^h-\phi_2^h,\psi_1^h-\psi_2^h\right)_{1,\Omega_O}+\omega_{\mathbf{v}}\left(\mathbf{u}_1^h-\mathbf{u}_2^h,\mathbf{v}_1^h-\mathbf{v}_2^h\right)_{\mathrm{div},\Omega_O}
\end{aligned}
\tag{13}
$$

and $F^h_\Sigma(\{\psi^h,\mathbf{v}^h\})=\sum_i(f_i,\nabla\cdot\mathbf{v}_i^h)_{0,\Omega_i^h}+(f_i,\psi_i^h)_{0,\Omega_i^h}$, respectively.

The next section justifies the choice $\omega_\phi=\omega_{\mathbf{v}}=3$.

3 Analysis of the mesh tying LSFEM

When the mesh tying region Σ^h is such that $\sigma^h\neq\emptyset$, the least-squares functional (10) is mesh dependent. The proofs in [6] can be modified to show that (10) is norm equivalent on $\mathbf{H}^h$. However, the mesh dependence of this functional prevents it from being norm-equivalent on the space $\mathbf{H}$. Consequently, the bilinear form B^h_Σ is coercive only on $\mathbf{H}^h\times\mathbf{H}^h$.

In this section we will assume that Σ^h consists only of an overlap region Ω_O and that $\sigma^h=\emptyset$. In this case the least-squares functional (10) is not mesh-dependent and one can show that it is norm-equivalent on $\mathbf{H}$. As a result, B^h_Σ is coercive on $\mathbf{H}\times\mathbf{H}$. This implies that for mesh-tying problems there's no reward for perturbing the discrete interfaces to match exactly. In the contrary, volume coupling gives rise to a least-squares functional with a better norm-equivalence properties than surface coupling. The explanation is that the mesh-dependent terms in (10) approximate norms in $H^{1/2}(\sigma^h)$ and $H^{-1/2}(\sigma^h)$ by weighted L^2 norms on σ. It is well-known that weighted L^2 norms are not spectrally equivalent to the true norms and so, the norm-equivalence is possible only for discrete spaces [5].

We will prove norm-equivalence of the mesh-tying least-squares functional with respect to the following energy norm

$$
\begin{aligned}
|||\{\psi,\mathbf{v}\}|||^2=\sum_{i=1}^{2}&\left(\|\mathbf{v}_i\|^2_{\mathrm{div},\Omega_i^h}+\|\psi_i\|^2_{1,\Omega_i^h}\right)\\
&+\|\psi_1-\psi_2\|^2_{1,\Omega_O}+\|\mathbf{v}_1-\mathbf{v}_2\|^2_{\mathrm{div},\Omega_O}\,.
\end{aligned}
\tag{14}
$$

Our proof uses the trace inequalities that for every $\psi \in H^1(\mathcal{D})$ and $\mathbf{v} \in H(\mathrm{div}, \mathcal{D})$

$$\|\psi\|_{1/2,\partial\mathcal{D}} \leq \|\psi\|_{1,\mathcal{D}} \quad \text{and} \quad \|\mathbf{v}\|_{-1/2,\partial\mathcal{D}} \leq \|\mathbf{v}\|_{\mathrm{div},\mathcal{D}}\,, \tag{15}$$

and Green's identity [14, p.28],

$$(\mathbf{v}, \nabla\psi)_{0,\mathcal{D}} + (\nabla\cdot\mathbf{v}, \psi)_{0,\mathcal{D}} = \langle \mathbf{v}\cdot\mathbf{n}, \psi\rangle_{\partial\mathcal{D}}\,. \tag{16}$$

Theorem 1 *There exist positive weights ω_ϕ, $\omega_{\mathbf{v}}$, independent of the maximum element diameter h, such that for every $\{\psi, \mathbf{v}\} \in \mathbf{H}$ there holds the lower bound*

$$J_h(\{\psi, \mathbf{v}\}; 0) \geq \frac{1}{4}|||\{\psi, \mathbf{v}\}|||^{\mathbf{2}}\,. \tag{17}$$

The coercivity of (13) on $\mathbf{H}\times\mathbf{H}$ is a corollary of Theorem 1.

Corollary 2 *In the notation of Theorem 1, for every $\{\phi, \mathbf{u}\}, \{\psi, \mathbf{v}\} \in \mathbf{H}$*

$$\frac{1}{4}|||\{\phi, \mathbf{u}\}|||^2 \leq B^h_\Sigma(\{\phi, \mathbf{u}\}, \{\phi, \mathbf{u}\}) \tag{18}$$

and

$$B^h_\Sigma(\{\phi, \mathbf{u}\}, \{\psi, \mathbf{v}\}) \leq |||\{\phi, \mathbf{u}\}||| \cdot |||\{\psi, \mathbf{v}\}|||^2\,. \tag{19}$$

Proof of Corollary 2. *Equation (18) follows from the identity*

$$J_h(\{\phi, \mathbf{u}\}; 0) = B^h_\Sigma(\{\phi, \mathbf{u}\}, \{\phi, \mathbf{u}\})$$

and the norm-equivalence (17). Continuity follows by a repeated application of the Cauchy's inequality and the definition of the mesh-tying energy norm.

Proof of Theorem 1. *After expanding terms in* (10)

$$\begin{aligned} J_h(\{\psi, \mathbf{v}\}; 0) = &\sum_{i=1}^{2} \left(\|\nabla\cdot\mathbf{v}_i\|^2_{0,\Omega^h_i} + \|\mathbf{v}_i\|^2_{0,\Omega^h_i} + \|\nabla\psi_i\|^2_{0,\Omega^h_i} + \|\psi_i\|^2_{0,\Omega^h_i}\right) \\ &+2\sum_{i=1}^{2}\int_{\Omega^h_i} \nabla\cdot\mathbf{v}_i\psi_i\,dx + \int_{\Omega^h_i}\mathbf{v}_i\cdot\nabla\psi_i\,dx + \omega_\phi\|\psi_1-\psi_2\|_{1,\Omega_O} + \omega_v\|\mathbf{v}_1-\mathbf{v}_2\|^2_{\mathrm{div},\Omega_O}. \end{aligned}$$

The norm definition (3)-(4) and Green's identity (16) give

$$J_h(\{\psi,\mathbf{v}\};0)=\sum_{i=1}^{2}\left(\|\mathbf{v}_i\|^2_{\mathrm{div},\Omega_i^h}+\|\psi_i\|^2_{0,\Omega_i^h}+2\int\limits_{\partial\Omega_i^h}\psi_i\mathbf{v}_i\cdot\mathbf{n}\,ds\right)$$
$$+\omega_\phi\|\psi_1-\psi_2\|_{1,\Omega_O}+\omega_v\|\mathbf{v}_1-\mathbf{v}_2\|^2_{\mathrm{div},\Omega_O}\,.$$

Note that $\partial\Omega_i^h=\sigma_i^h\cup\Gamma_i$ and $\psi_i=0$ on the Dirichlet boundary Γ_i. Therefore,

$$\int\limits_{\partial\Omega_i^h}\psi_i\mathbf{v}_i\cdot\mathbf{n}\,dx=\int\limits_{\sigma_i^h}\psi_i\mathbf{v}_i\cdot\mathbf{n}_i\,dx\,,$$

where $\mathbf{n}_i$ is the normal on σ_i^h that coincides with the outer normal on $\partial\Omega_i^h$. By adding and subtracting ψ_2 and $\mathbf{v}_2$ to the integral along σ_1^h, we write it as

$$\int\limits_{\sigma_1^h}\psi_1\mathbf{v}_1\cdot\mathbf{n}\,ds=\frac{1}{2}\left\{\int\limits_{\sigma_1^h}(\psi_1-\psi_2)\mathbf{v}_1\cdot\mathbf{n}_1\,ds+\int\limits_{\sigma_1^h}\psi_1(\mathbf{v}_1-\mathbf{v}_2)\cdot\mathbf{n}_1\,ds\right\}$$
$$+\frac{1}{2}\left\{\int\limits_{\sigma_1^h}\psi_2\mathbf{v}_1\cdot\mathbf{n}_1\,ds+\int\limits_{\sigma_1^h}\psi_1\mathbf{v}_2\cdot\mathbf{n}_1\,ds\right\}\,.$$

Similarly for the integral along σ_2^h we add and subtract ψ_1 and $\mathbf{v}_1$:

$$\int\limits_{\sigma_2^h}\psi_2\mathbf{v}_2\cdot\mathbf{n}\,ds=\frac{1}{2}\left\{\int\limits_{\sigma_2^h}(\psi_2-\psi_1)\mathbf{v}_2\cdot\mathbf{n}_2\,ds+\int\limits_{\sigma_2^h}\psi_2(\mathbf{v}_2-\mathbf{v}_1)\cdot\mathbf{n}_2\,ds\right\}$$
$$+\frac{1}{2}\left\{\int\limits_{\sigma_2^h}\psi_1\mathbf{v}_2\cdot\mathbf{n}_2\,ds+\int\limits_{\sigma_2^h}\psi_2\mathbf{v}_1\cdot\mathbf{n}_2\,ds\right\}\,.$$

Using that $\partial\Omega_O=\sigma_1^h\cup\sigma_2^h$ gives

$$\int\limits_{\sigma_1^h}\psi_2\mathbf{v}_1\cdot\mathbf{n}_1\,ds+\int\limits_{\sigma_1^h}\psi_1\mathbf{v}_2\cdot\mathbf{n}_1\,ds+\int\limits_{\sigma_2^h}\psi_1\mathbf{v}_2\cdot\mathbf{n}_2\,ds+\int\limits_{\sigma_2^h}\psi_2\mathbf{v}_1\cdot\mathbf{n}_2\,ds$$
$$=\int\limits_{\partial\Omega_O}\psi_2\mathbf{v}_1\cdot\mathbf{n}\,ds+\int\limits_{\partial\Omega_O}\psi_1\mathbf{v}_2\cdot\mathbf{n}\,ds\,.$$

Using the Green's formula (16) gives the identities

$$\int\limits_{\partial\Omega_O}\psi_2\mathbf{v}_1\cdot\mathbf{n}\,ds=\frac{1}{2}\Big\{\|\nabla\cdot\mathbf{v}_1+\psi_2\|_{0,\Omega_O}+\|\nabla\psi_2+\mathbf{v}_1\|_{0,\Omega_O}-\|\mathbf{v}_1\|^2_{\mathrm{div},\Omega_O}-\|\psi_2\|^2_{1,\Omega_O}\Big\}$$

and

$$\int_{\partial\Omega_O} \psi_1 \mathbf{v}_2 \cdot \mathbf{n}\, ds = \frac{1}{2}\Big\{ \|\nabla\cdot\mathbf{v}_2 + \psi_1\|_{0,\Omega_O} + \|\nabla\psi_1 + \mathbf{v}_2\|_{0,\Omega_O} - \|\mathbf{v}_2\|^2_{\mathrm{div},\Omega_O} - \|\psi_1\|^2_{1,\Omega_O} \Big\}.$$

Therefore, the least-squares functional can be written as

$$\begin{aligned} J_h(\psi, \mathbf{v}; 0) = &\sum_{i=1}^{2} \left(\|\mathbf{v}_i\|^2_{\mathrm{div},\Omega_i^h} + \|\psi_i\|^2_{0,\Omega_i^h} \right) - \frac{1}{2} \sum_{i=1}^{2} \left(\|\mathbf{v}_i\|^2_{\mathrm{div},\Omega_O} + \|\psi_i\|^2_{1,\Omega_O} \right) \\ &+ \omega_\phi \|\psi_1 - \psi_2\|_{1,\Omega_O} + \omega_v \|\mathbf{v}_1 - \mathbf{v}_2\|^2_{\mathrm{div},\Omega_O} \\ &+ \frac{1}{2}\Big\{ \|\nabla\cdot\mathbf{v}_1 + \psi_2\|_{0,\Omega_O} + \|\nabla\psi_2 + \mathbf{v}_1\|_{0,\Omega_O} \\ &\quad + \|\nabla\cdot\mathbf{v}_2 + \psi_1\|_{0,\Omega_O} + \|\nabla\psi_1 + \mathbf{v}_2\|_{0,\Omega_O} \\ &\quad + \int_{\sigma_1^h} (\psi_1 - \psi_2)\mathbf{v}_1 \cdot \mathbf{n}_1\, ds + \int_{\sigma_1^h} \psi_1(\mathbf{v}_1 - \mathbf{v}_2)\cdot\mathbf{n}_1\, ds \\ &\quad + \int_{\sigma_2^h} (\psi_2 - \psi_1)\mathbf{v}_2 \cdot \mathbf{n}_2\, ds + \int_{\sigma_2^h} \psi_2(\mathbf{v}_2 - \mathbf{v}_1)\cdot\mathbf{n}_2\, ds \Big\}. \end{aligned}$$

To obtain a lower bound for the least-squares functional we drop the (non-negative) norm terms inside the curly braces. Because $\Omega_O \subset \Omega_i^h$ we have that

$$\frac{1}{2} \sum_{i=1}^{2} \left(\|\mathbf{v}_i\|^2_{\mathrm{div},\Omega_O} + \|\psi_i\|^2_{1,\Omega_O} \right) \le \frac{1}{2} \sum_{i=1}^{2} \left(\|\mathbf{v}_i\|^2_{\mathrm{div},\Omega_i^h} + \|\psi_i\|^2_{1,\Omega_i^h} \right).$$

The first integral inside the curly braces is estimated as follows:

$$\begin{aligned} &\left| \int_{\sigma_1^h} (\psi_1 - \psi_2)\mathbf{v}_1 \cdot \mathbf{n}_1\, dx \right| \\ &\quad \le \|\psi_1 - \psi_2\|_{1/2,\sigma_1^h} \|\mathbf{v}_1 \cdot \mathbf{n}\|_{-1/2,\sigma_1^h} && \text{using duality} \\ &\quad \le \|\psi_1 - \psi_2\|_{1/2,\partial\Omega_O} \|\mathbf{v}_1 \cdot \mathbf{n}\|_{-1/2,\partial\Omega_O} && \text{using } \partial\Omega_O = \sigma_1^h \cup \sigma_2^h \\ &\quad \le \|\psi_1 - \psi_2\|_{1,\Omega_O} \|\mathbf{v}_1\|_{\mathrm{div},\Omega_O} && \text{using trace inequalities (15)} \\ &\quad \le \frac{1}{4\epsilon_1} \|\psi_1 - \psi_2\|^2_{1,\Omega_O} + \epsilon_1 \|\mathbf{v}_1\|^2_{\mathrm{div},\Omega_O} && \text{using the } \epsilon\text{-inequality}. \end{aligned}$$

The remaining three integrals are estimated using the same inequalities:

$$\left| \int_{\sigma_1^h} \psi_1(\mathbf{v}_1 - \mathbf{v}_2)\cdot\mathbf{n}_1\, dx \right| \le \epsilon_2 \|\psi_1\|^2_{1,\Omega_O} + \frac{1}{4\epsilon_2} \|\mathbf{v}_1 - \mathbf{v}_2\|^2_{\mathrm{div},\Omega_O};$$

$$\left| \int_{\sigma_2^h} (\psi_2 - \psi_1)\mathbf{v}_2 \cdot \mathbf{n}_2 \, dx \right| \leq \frac{1}{4\epsilon_3} \|\psi_2 - \psi_1\|^2_{1,\Omega_O} + \epsilon_3 \|\mathbf{v}_2\|^2_{\mathrm{div},\Omega_O} ;$$

$$\left| \int_{\sigma_2^h} \psi_2(\mathbf{v}_2 - \mathbf{v}_1) \cdot \mathbf{n}_2 \, dx \right| \leq \epsilon_4 \|\psi_2\|^2_{1,\Omega_O} + \frac{1}{4\epsilon_4} \|\mathbf{v}_2 - \mathbf{v}_1\|^2_{\mathrm{div},\Omega_O} .$$

For $\epsilon_i = 1/4$, $1 \leq i \leq 4$, all the bounds combined yield

$$J_h\{\psi, \mathbf{v}\}; 0 \geq \frac{1}{4} \sum_{i=1}^{2} \left(\|\mathbf{v}_i\|^2_{\mathrm{div},\Omega_i^h} + \|\psi_i\|^2_{0,\Omega_i^h} \right) + (\omega_\phi - 2)\|\psi_1 - \psi_2\|_{1,\Omega_O} + (\omega_{\mathbf{v}} - 2)\|\mathbf{v}_1^h - \mathbf{v}_1^h\|_{\mathrm{div},\Omega_O} .$$

By choosing $\omega_\phi = \omega_{\mathbf{v}} = 3$ the inequality (17) holds.

3.1 Error estimates

Throughout this section ψ_i and $\mathbf{v}_i$ will stand for the restrictions of functions $\psi \in H_0^1(\Omega)$ and $\mathbf{v} \in H(\mathrm{div}, \Omega)$ to the subdomains Ω_h^i. According to the assumption in (2), the closure of each subdomain is contained in Ω and so, ψ_i and $\mathbf{v}_i$ are well-defined.

We assume that $\mathbf{H}^h = \Phi_r^h \times \mathbf{V}_p^h$ where the finite element spaces

$$\Phi_r^h = \Phi_{r,1}^h \times \Phi_{r,2}^h; \quad \Phi_{r,i}^h \subset H_\Gamma^1(\Omega_i^h), \ i = 1, 2 ;$$

$$\mathbf{V}_p^h = \mathbf{V}_{p,1}^h \times \mathbf{V}_{p,2}^h; \quad \mathbf{V}_{p,i}^h \subset H(\mathrm{div}, \Omega_i^h), \ i = 1, 2$$

have the following approximation properties. For every $\psi \in H^{r+1}(\Omega)$ there exists $\psi^h = (\psi_1^h, \psi_2^h) \in \Phi_r^h$ such that

$$\sum_{i=1}^{2} \|\psi_i - \psi_i^h\|_{0,\Omega_i^h} + h|\psi_i - \psi_i^h|_{1,\Omega_i^h} \leq Ch^{r+1}\|\psi\|_{r+1,\Omega} \tag{20}$$

and for every $\mathbf{v} \in H(\mathrm{div}, \Omega) \cap (H^{p+1}(\Omega))^2$ there exists $\mathbf{v}^h = (\mathbf{v}_1^h, \mathbf{v}_2^h) \in \mathbf{V}_p^h$ such that

$$\sum_{i=1}^{2} \|\mathbf{v}_i - \mathbf{v}_i^h\|_{0,\Omega_i^h} + h\|\nabla \cdot (\mathbf{v}_i - \mathbf{v}_i^h)\|_{0,\Omega_i^h} \leq Ch^{p+1}\|\mathbf{v}\|_{p+1,\Omega} . \tag{21}$$

The error bound (20) holds for standard C^0 piecewise polynomial spaces of order r. The error bound (21) is valid for C^0 spaces of order p and certain $H(\mathrm{div}, \Omega)$ conforming spaces such as BDM_p.

Theorem 3 *Assume that the first order system*

$$\begin{cases} \nabla \cdot \mathbf{u} + \phi = f \quad \textit{and} \quad \nabla\phi + \mathbf{u} = 0 \quad \textit{in } \Omega \\ \phi = 0 \quad \textit{on } \partial\Omega \end{cases}$$

has a solution $\phi \in H_0^1(\Omega) \cap H^{r+1}(\Omega)$ *and* $\mathbf{u} \in H(\mathrm{div}, \Omega) \cap (H^{p+1}(\Omega))^2$. *If* $\{\phi^h, \mathbf{u}^h\} \in \mathbf{H}^h$ *is a solution of the least-squares mesh-tying problem (12), then*

$$|||\{\phi - \phi^h, \mathbf{u} - \mathbf{u}^h\}||| \leq C \left(h^r \|\phi\|_{r+1,\Omega} + h^p \|\mathbf{u}\|_{p+1,\Omega}\right) . \tag{22}$$

Proof. *Clearly, for the restrictions* ϕ_i *and* $\mathbf{u}_i$ *of* ϕ *and* $\mathbf{u}$ *there holds*

$$\nabla \cdot \mathbf{u}_i + \phi_i = f_i \ \textit{in } \Omega_i \quad \textit{and} \quad \nabla\phi_i + \mathbf{u}_i = 0 \ \textit{in } \Omega_i \, .$$

Using this and the fact that $\phi_1 = \phi_2$ *and* $\mathbf{u}_1 = \mathbf{u}_2$ *on* Ω_O,

$$\begin{aligned} \sum_{i=1}^{2} \left(\nabla \cdot \mathbf{u}_i + \phi_i - f_i, \nabla \cdot \mathbf{v}_i^h + \psi_i^h\right)_{0,\Omega_i^h} + \left(\nabla\phi_i + \mathbf{u}_i, \nabla\psi_i^h + \mathbf{v}_i^h\right)_{0,\Omega_i^h} \\ + \left(\phi_1 - \phi_2, \psi_1^h - \psi_2^h\right)_{1,\Omega_O} + \left(\mathbf{u}_1 - \mathbf{u}_2, \mathbf{v}_1^h - \mathbf{v}_2^h\right)_{\mathrm{div},\Omega_O} = 0 \end{aligned} \tag{23}$$

for all $\{\psi^h, \mathbf{v}^h\} \in \mathbf{H}^h$. *Equivalently,*

$$B_\Sigma^h(\{\phi, \mathbf{u}\}, \{\psi^h, \mathbf{v}^h\}) = F_\Sigma^h(\{\psi^h, \mathbf{v}^h\}) \quad \forall \{\psi^h, \mathbf{v}^h\} \in \mathbf{H}^h \, .$$

Subtracting from (12) gives the error orthogonality equation

$$B_\Sigma^h(\{\phi - \phi^h, \mathbf{u} - \mathbf{u}^h\}, \{\psi^h, \mathbf{v}^h\}) = 0 \quad \forall \{\psi^h, \mathbf{v}^h\} \in \mathbf{H}^h \, .$$

Coercivity (18), continuity (19) of B_Σ^h *and orthogonality imply*

$$\begin{aligned} \frac{1}{4}|||\{\phi - \phi^h, \mathbf{u} - \mathbf{u}^h\}|||^2 &\leq B_\Sigma^h(\{\phi - \phi^h, \mathbf{u} - \mathbf{u}^h\}, \{\phi - \phi^h, \mathbf{u} - \mathbf{u}^h\}) \\ &= B_\Sigma^h(\{\phi - \phi^h, \mathbf{u} - \mathbf{u}^h\}, \{\phi - \psi^h, \mathbf{u} - \mathbf{v}^h\}) \\ &\leq |||\{\phi - \phi^h, \mathbf{u} - \mathbf{u}^h\}||| \, |||\{\phi - \psi^h, \mathbf{u} - \mathbf{v}^h\}||| \end{aligned}$$

where $\{\psi^h, \mathbf{v}^h\} \in \mathbf{H}^h$ *is arbitrary. Therefore,*

$$\frac{1}{4}|||\{\phi - \phi^h, \mathbf{u} - \mathbf{u}^h\}||| \leq \inf_{\{\psi^h, \mathbf{v}^h\} \in \mathbf{H}^h} |||\{\phi - \psi^h, \mathbf{u} - \mathbf{v}^h\}||| \, .$$

The theorem follows by noting that

$$|||\{\phi - \psi^h, \mathbf{u} - \mathbf{v}^h\}||| \leq 2 \sum_{i=1}^{2} \|\mathbf{u}_i - \mathbf{v}_i^h\|_{\mathrm{div},\Omega_i^h} + \|\phi_i - \psi_i^h\|_{1,\Omega_i^h}$$

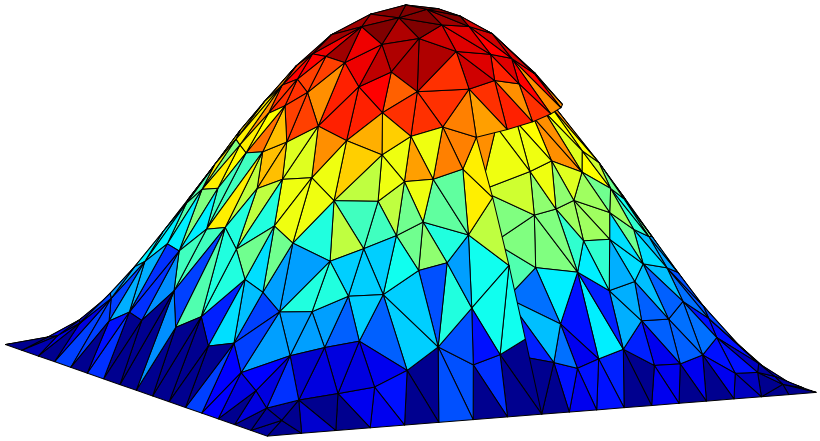

Fig. 3. Finite element approximation of the manufactured solution $\phi(x,y) = \cos(\frac{\pi x}{2})\cos(\frac{\pi y}{2})$ by the least-squares mesh-tying method using the overlapping subdomains from Figure 2.

and using the approximation hypotheses (20)-(21).

We note that the estimate (22) implies that the LSFEM passes a patch test of order $s = \min\{p, r\}$ by default.

4 Numerical results

In this section we study numerical convergence rates of the least-squares mesh-tying method (10), using the manufactured solution $\phi(x,y) = \cos(\frac{\pi x}{2})\cos(\frac{\pi y}{2})$ and $\Omega = [-1,1]^2$. The overlapping subdomains are as shown in Figure (2). The displacement ϕ and flux $\mathbf{u}$ are discretized using piecewise linear nodal shape functions, i.e , $r = p = 1$ in the definition of $\mathbf{H}^h$.

To estimate convergence rates we use a sequence of non-uniform (but uniformly regular) grids wish mesh parameter [6] h ranging from 0.75 to 0.02. The corresponding numbers of unknowns are 121 and 81200, respectively. The first half of the grids in the sequence (for h ranging from 0.75 to approximately 0.1) where generated using Triangle [21] with a uniform area constraint. The second half of the grids were obtained by applying uniform mesh refinement

[6] We define h to be the maximum element diameter in the mesh.

to the last grid from the first half of the sequence. The boundary nodes were snapped to the exact curved boundary.

In the following figures the red curves correspond to the left (red) subdomain Ω_1 in Figure 2. The green curves are associated with the right (green) subdomain Ω_2, in the same figure. Figure 3 shows a typical finite element solution by the LSFEM using overlapping subdomains of Ω. Convergence rates data is summarized in Figures 4-5.

For piecewise linear elements the estimate (22) from Theorem 3 specializes to

$$|||\{\phi - \phi^h, \mathbf{u} - \mathbf{u}^h\}||| \leq Ch$$

Thus, definition (14) of the energy norm $|||\{\phi, \mathbf{u}\}|||$ implies that the rates of convergence for the flux error in $H(\mathrm{div}, \Omega)$ and the displacement error in $H^1(\Omega)$ should equal one. The corresponding error plots in Figures 4-5 assert that these theoretical rates also hold numerically.

The error analysis in Theorem 3 does not include separate estimates for the L^2 errors in the flux and the displacement. Regarding the flux, note that $\mathbf{u} = -\nabla\phi$ and so, $|\phi_i^h - \phi_i|_1 \approx \|\mathbf{u}_i^h - \mathbf{u}_i\|_0$. As a result, we can expect that the flux approximation is first-order accurate in L^2. Figure 4 compares these two quantities and shows that this is indeed the case. For the L^2 error in the displacement we observed second order accuracy.

Studies of overlap region's width as a function of h, decreasing the width from $h/4$ down to h^2, were also performed. Convergence of $\|\nabla\cdot\mathbf{u}_i^h - \nabla\cdot\mathbf{u}_i\|_0$ was found to be independent of the overlap width. However, both the displacements H^1 semi-norm, $|\phi_i^h - \phi_i|_1$ and the fluxes L^2 norm, $\|\mathbf{u}_i^h - \mathbf{u}_i\|_0$ converged sublinearly (if at all) for overlap widths h^α with $\alpha > 1$.

The results here are consistent with those reported in [4], in which $\omega_\phi = \omega_{\mathbf{v}} = 3$ too. The examples reported there include linear patch tests, in which the computed displacements and fluxes differ with the corresponding exact only in the trailing bits of double precision arithmetic.

5 Conclusions

Mixed Galerkin methods for mesh tying that are consistent when applied to geometries with curved interfaces may significantly increase the complexity of the overall solution [17], and lead to indefinite linear systems [1–3, 15, 19]. We formulated and analyzed a LSFEM for mesh tying that is optimally accurate, patch test consistent for arbitrary order discretizations, and gives rise to sparse symmetric positive definite matrices. The method is formulated

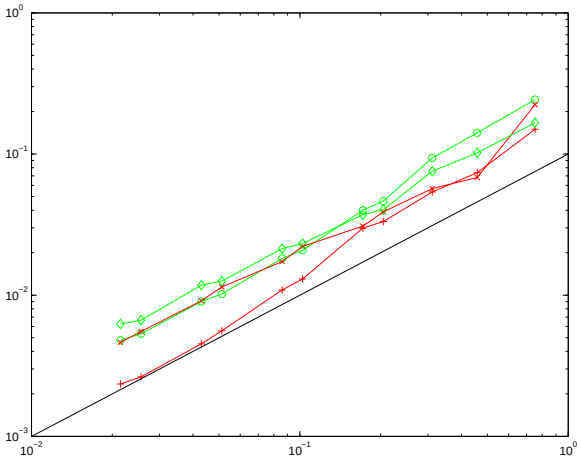

Fig. 4. Loglog plots of the errors $\|\mathbf{u}_i^h - \mathbf{u}_i\|_0$, and $|\phi_i^h - \phi|_1$ vs. h in each subdomain Ω_i. The red curves correspond to Ω_1 and the green curves correspond to Ω_2. The straight black line has slope 1. The curves marked with the red + and the green o are the H^1 semi-norms of the displacement errors in Ω_1 and Ω_2 respectively. The curves marked with the red $\times$ and the green diamond are the L^2 norms of the flux error in Ω_1 and Ω_2 respectively.

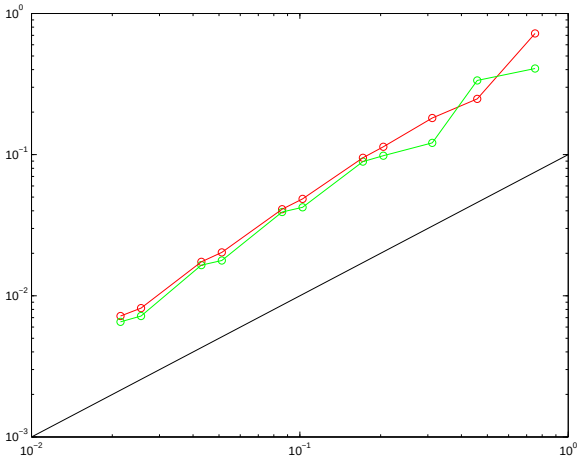

Fig. 5. Loglog plots of the error $\|\nabla \cdot \mathbf{u}_i^h - \nabla \cdot \mathbf{u}_i\|_0$ vs. h in each subdomain Ω_i. The red curve corresponds to Ω_1 and the green curve corresponds to Ω_2. The straight black line has slope 1. This quantity was observed to be independent of the width of the overlap region.

for overlapping domains; in the case of non-empty void regions application of least-squares is preceded by an interface perturbation step to close the voids. The use of least-squares is subject to certain tradeoffs, such as specialized $H(\mathrm{div}, \Omega)$ preconditioners, more variables [7], and need for intrusive refactoring of legacy codes.

[7] This ceases to be a drawback if the flux variable is of primary interest as in porous media flow applications.

Acknowledgments

The authors thank Misha Shaskov (LANL) and Pat Knupp (Sandia) for helpful discussions.

References

[1] I. Babuska and J.M. Melenk. The partition of unity method. *Int. J. Numer. Methods Engrg.*, 40:727–758, 1997.

[2] C. Bacuta and J. Sun. Partition of unity finite element method implementation for Poisson equation. In F. Liu, editor, *Advances in Applied and Computational Mathematics*, pages 35–46. Nova Publishers, 2006.

[3] H. Ben-Dia and G.Rateau. The Arlequin method as a flexible engineering design tool. *Int. J. Numer. Methods Engrg.*, 62:1442–1462, 2005.

[4] P. Bochev and D. M. Day. A least-squares method for consistent mesh tying. *Int. J. Num. Anal. and Modeling*, 4:342–352, 2007.

[5] P. Bochev and M. Gunzburger. Finite element methods of least-squares type. *SIAM Review*, 40(4):789–837, 1998.

[6] Y. Cao and M. Gunzburger. Least-squares finite element approximations to solutions of interface problems. *SIAM J. Numer. Anal.*, 35(1):393–405, 1998.

[7] G. Chesshire and W.D. Henshaw. Composite overlapping meshes for the solution of partial differential equations. *J. Comp. Phys.*, 90(1):1–64, 1990.

[8] C. R. Dohrmann, S. W. Key, and M. W. Heinstein. A method for connecting dissimilar finite element meshes in two dimensions. *Int. J. Numer. Methods Engrg.*, 48:655–678, 2000.

[9] C. R. Dohrmann, S. W. Key, and M. W. Heinstein. Methods for connecting dissimilar three-dimensional finite element meshes. *Int. J. Numer. Methods Engrg.*, 47:1057–1080, 2000.

[10] B. Flemisch, J.M. Melenk, and B.I. Wohlmuth. Mortar methods with curved interfaces. *Appl. Numer. Math.*, 54(3-4):339–361, 2005.

[11] B. Flemisch, M.A. Puso, and B.I. Wohlmuth. A new dual mortar method for curved interfaces: 2D elasticity. *Int. J. Numer. Methods Engrg.*, 63(6):813–832, 2005.

[12] B. Flemisch and B. I. Wohlmuth. Stable Lagrange multipliers for quadrilateral meshes of curved interfaces in 3D. *Comput. Meth. Appl. Mech. Engrg.*, 196(8):1589–1602, 2007.

[13] R. Garimella, M. Shashkov, and P. Knupp. Triangular and quadrilateral surface mesh quality optimization using local parametrization. *Comput. Meth. Appl. Mech. Engrg.*, 193:913–928, 2004.

[14] V. Girault and P. Raviart. *Finite Element Methods for Navier-Stokes Equations*. Springer, Berlin, 1986.

[15] P.-A. Guidault and T. Belytschko. On the L_2 and the H^1 couplings for an overlapping domain decomposition method using Lagrange multipliers. *Int. J. Numer. Methods Engrg.*, 2007. to appear.

[16] M. Holst. Applications of domain decomposition and partition of unity methods in physics and geometry (plenary paper). In I. Herrera, D.E. Keyes, O.B. Widlund, and R. Yates, editors, *Proceedings of the 14th International Conference on Domain Decomposition Methods*, pages 63–78, Cocoyoc, Mexico, 2002. UNAM.

[17] T. Laursen and M. Heinstein. A three dimensional surface-to-surface projection algorithm for non-coincident domains. *Comm. Num. Meth. Engrg.*, 19:421–432, 2003.

[18] T. A. Laursen and M. W. Heinstein. Consistent mesh tying methods for topologically distinct discretized surfaces in non-linear solid mechanics. *Int. J. Numer. Methods Engrg.*, 57:1197–1242, 2003.

[19] M. L. Parks, L. A. Romero, , and Pavel B. Bochev. A novel Lagrange-multiplier based method for consistent mesh tying. *Comput. Meth. Appl. Mech. Engrg.*, 2007. Accepted.

[20] N. A. Petersson. An algorithm for assembling overlapping grid systems. *SIAM J. Sci. Comput.*, 20:1995–2022, 1999.

[21] J.R. Shewchuk. Delaunay refinement algorithms for triangular mesh generation. *Computational Geometry: Theory and Applications*, 22:21–74, 2002.

[22] G. Strang and G. Fix. *An analysis of the finite element method*. Prentice Hall, New Jersy, 1973.

[23] A. Toselli and O. Widlund. *Domain decomposition methods - algorithms and theory*. Springer Verlag, 2005.